Directing cell migration and organization via nanocrater-patterned cell-repellent interfaces

Hojeong Jeon [1,2§], Sangmo Koo [1§], Willie Mae Reese [3], Peter Loskill,[3, 4] Costas P. Grigoropoulos [1*], and Kevin E. Healy [3, 4*]

[1] Laser Thermal Laboratory, Department of Mechanical Engineering, University of California, Berkeley, CA 94720, USA

[2] Center for Biomaterials, Biomedical Research Institute, Korea Institute of Science and Technology, Seoul 136-791, Republic of Korea

[3] Department of Materials Science and Engineering, University of California, Berkeley, CA 94720, USA

[4] Department of Bioengineering, and California Institute for Quantitative Biosciences (QB3), University of California at Berkeley, Berkeley, California 94720

[§]These authors contributed equally to this work.
To whom correspondence should be addressed.
Email: kehealy@berkeley.edu, cgrigoro@me.berkeley.edu

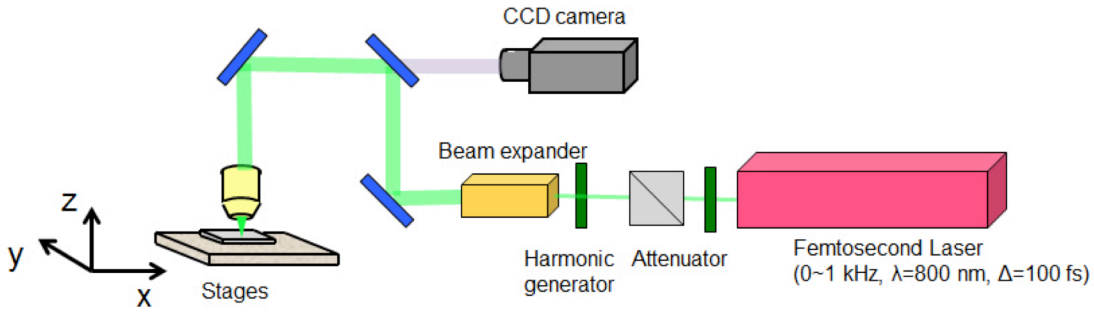

Figure S1. Schematic representation of the experimental setup used for laser ablation nanofabrication.

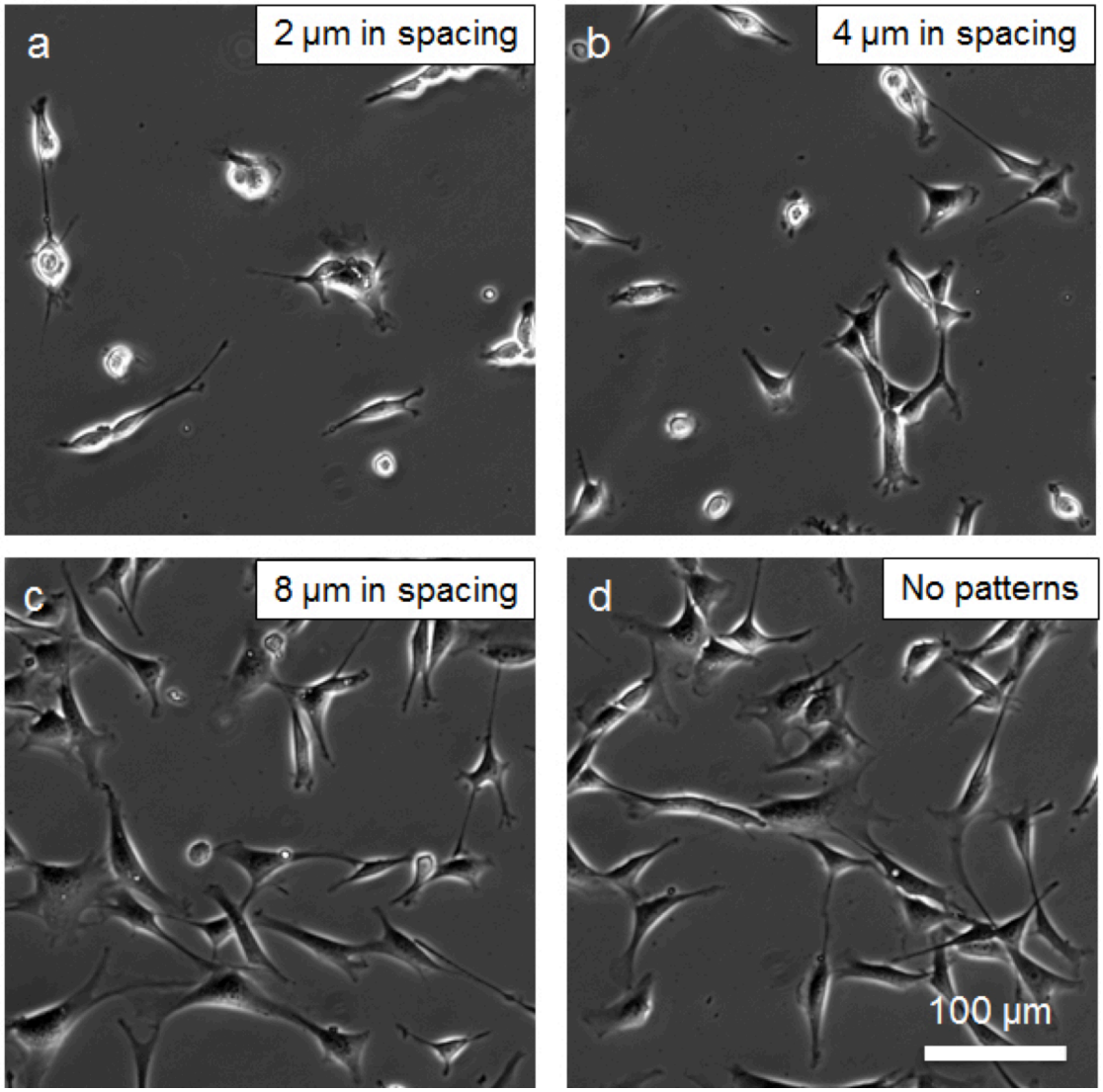

Figure S2. The nanocrater pattern spacing alters cell adhesion and morphology. Cells were plated on the nanocrater-patterned quartz surfaces in serum-containing medium for 15 hours. Fibroblasts attach and spread on patterned surfaces with craters (1 μm in diameter, 350 nm in depth) and **a,** 2 μm , **b,** 4 μm, **c,** 8 μm isometric spacing (i.e., pitch), and **d**, unpatterned surface. As the pitch decreased the number and degree of multiaxial spreading of the cells decreased. On the minimum pitch surfaces, refractile cells appear to be poorly spread and weakly attached.

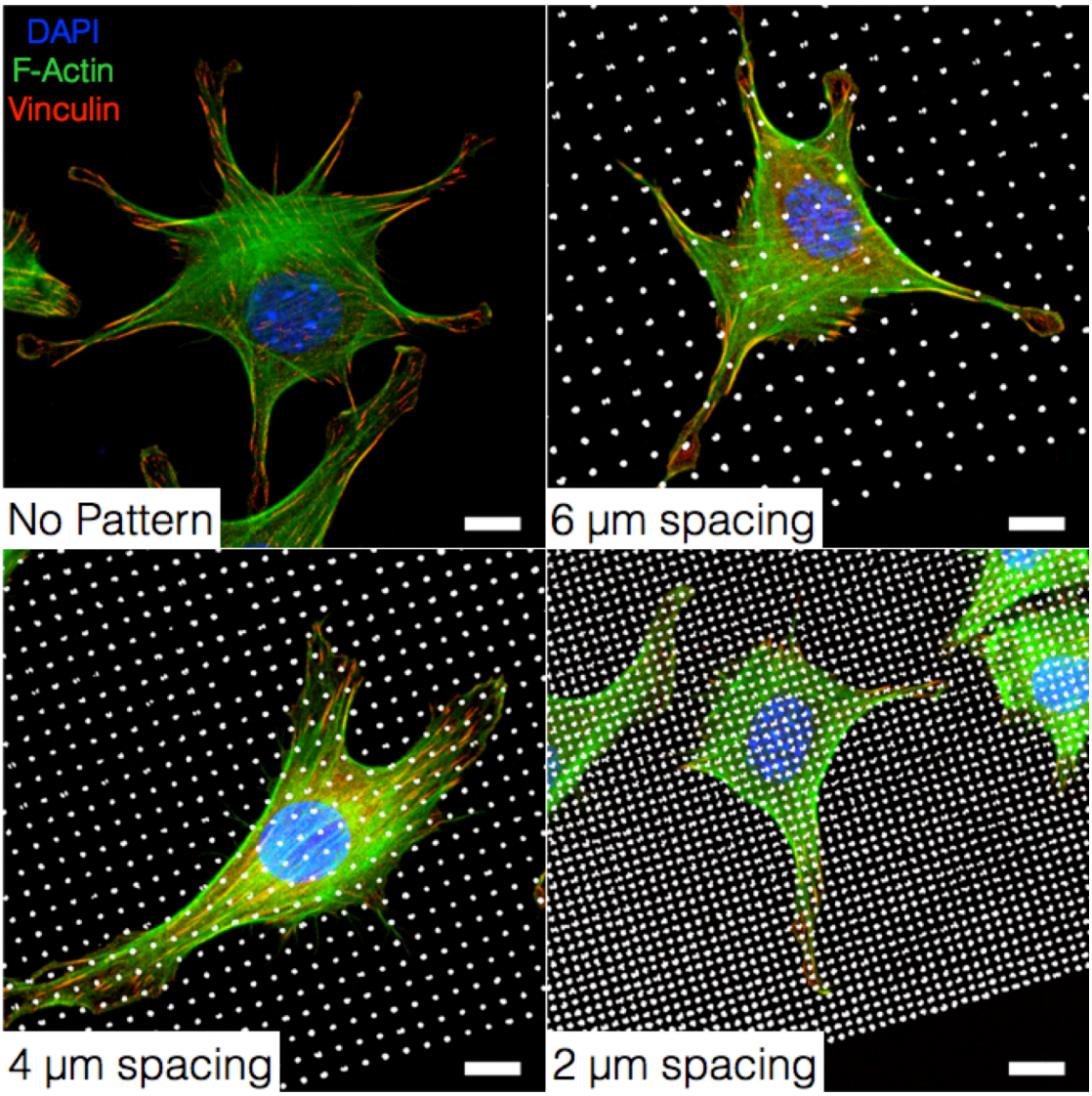

Figure S3. The nanocraters distort the cells' ability to form focal adhesions. Immunofluorescence images of fibroblast cultured on patterned quartz surfaces with craters (1 μm in diameter, 350 nm in depth) and unpatterned surface, 6 μm, 4 μm and 2 μm isometric spacing with inverted DIC. The cells were plated on the patterned surfaces in serum-containing medium for 1 hour. Depending on pattern pitch, cells reveal different morphology and focal adhesion distribution, where cells on surfaces with the lowest pitch have smaller and less pronounced focal adhesions that are primarily distributed at the leading and trailing edges of cells. Focal adhesions located on low pitch area or near nanocraters look nascent while larger and mature focal adhesions were located in on the planar "pitch" of the nanocraters. In contrast, focal adhesions of the cells on flat surfaces (no patterns) were scattered throughout the cell body. Scale bars =10 μm.

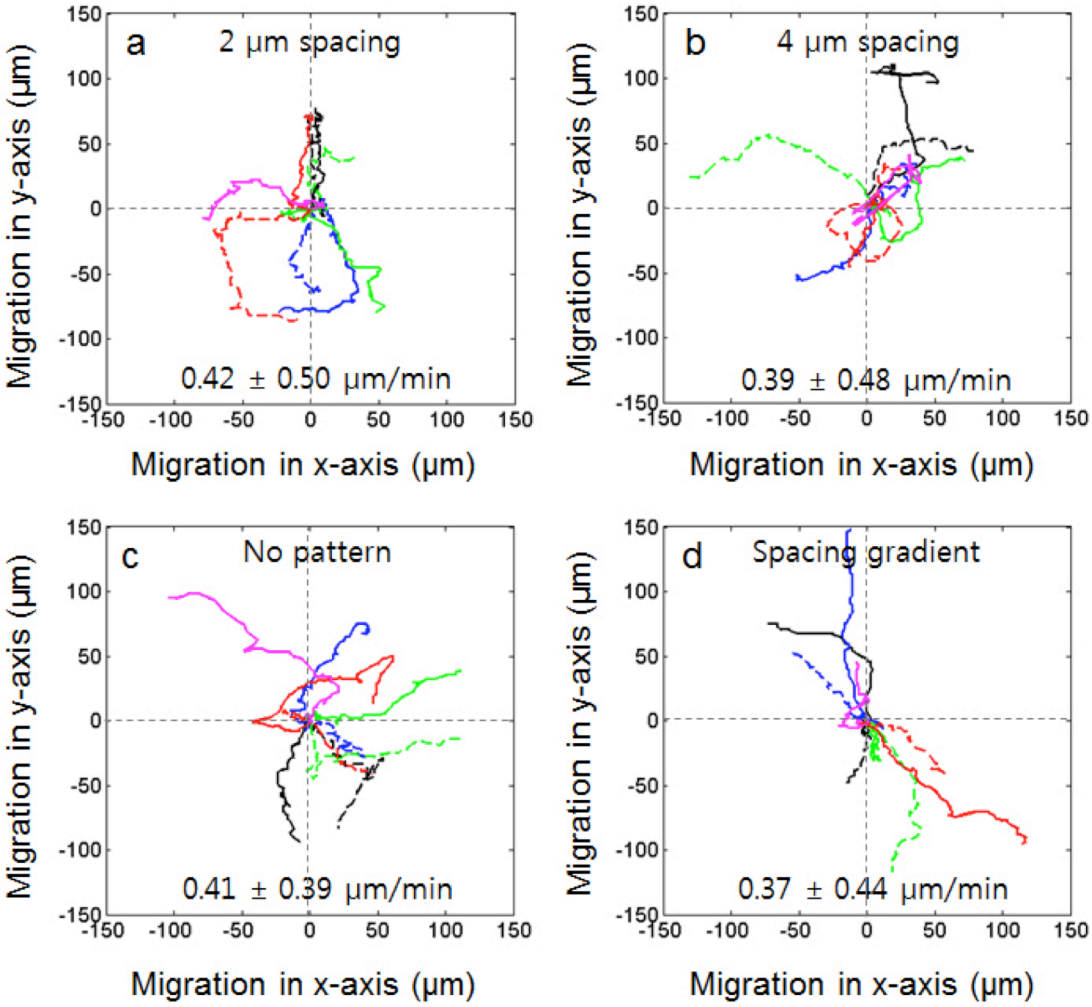

Figure S4. Trajectories of cell migration on isometric pitch (2 and 4 μm) patterns and a gradient (2, 3, and 4 μm) pattern with 800-nm diameter and 300-nm depth nanocraters in the quartz surface. Ten random cells were chosen to display cell migration on the patterned surfaces for ~7 hours after the cells attached to the surface and started to spread (~3 hours after cell seeding). The 10 traced lines, which are composed of two types of lines (solid and dash) with 5 colors (black, red, cyan, blue, and green) for each line, provide the transient migration characteristic depending on the pattern spacing. **a-c,** On the 2-μm and 4-μm pitch patterns and the flat surface, no specific directionality of cells was observed. **d,** On the other hand, the cells on the spacing gradient pattern maintained their linear direction and speed for extended time. For the spacing gradient pattern, the spacing was 3 μm (no gradient) for the x-axis, and the spacing in the y-axis was from 2 μm to 4 μm. The numbers in each graph show the averaged migration speed of the cells.

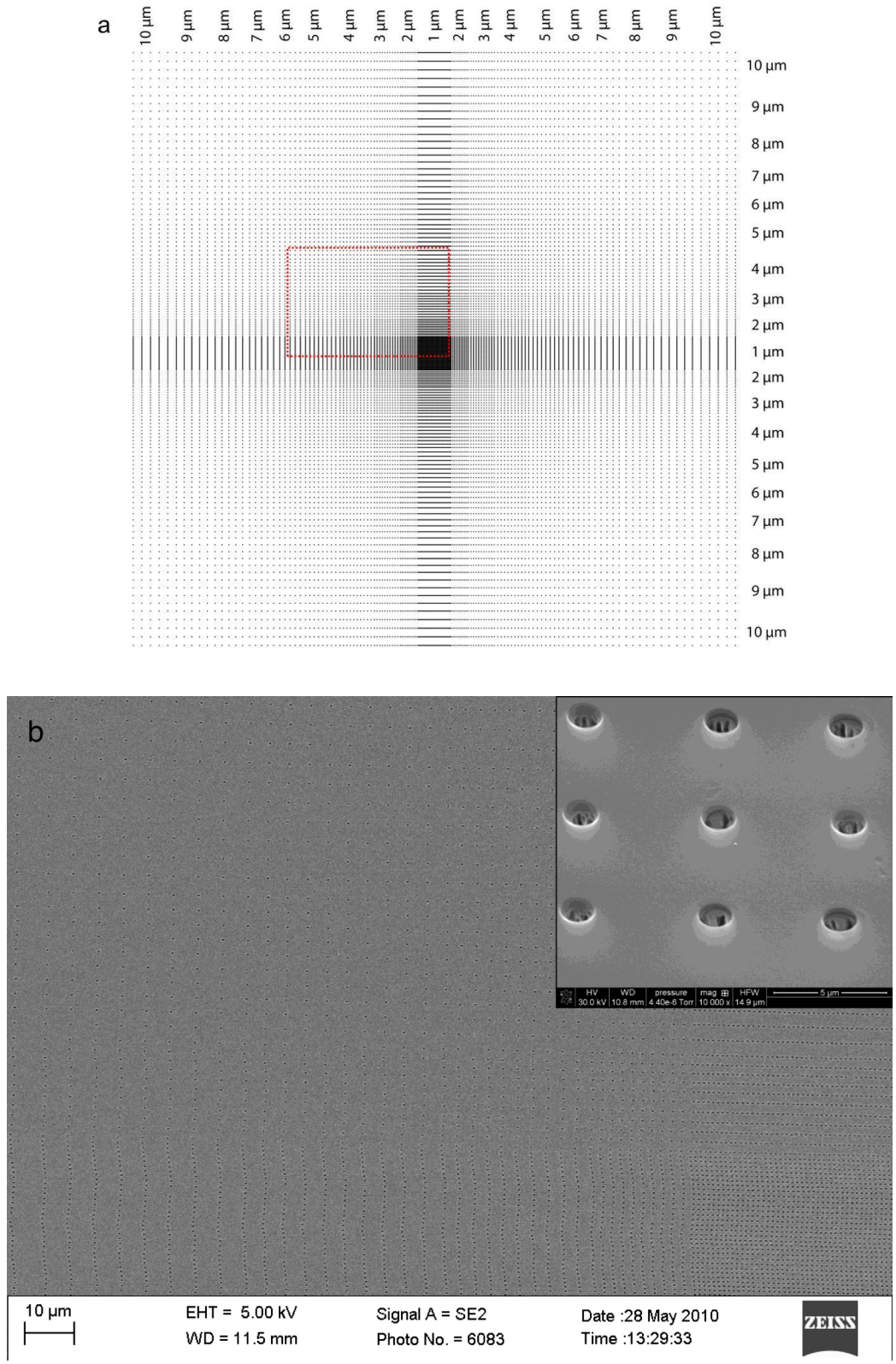

Figure S5. Gradient pattern. **a**, Diagram of gradient pattern used in this work. Block dots indicate the nanoscale craters and pitch dimensions, center-to-center distance between each crater, are given adjacent to the pattern border. **b**, SEM image of the dotted line box in Fig. S5a. Inset image shows higher magnification of the craters.

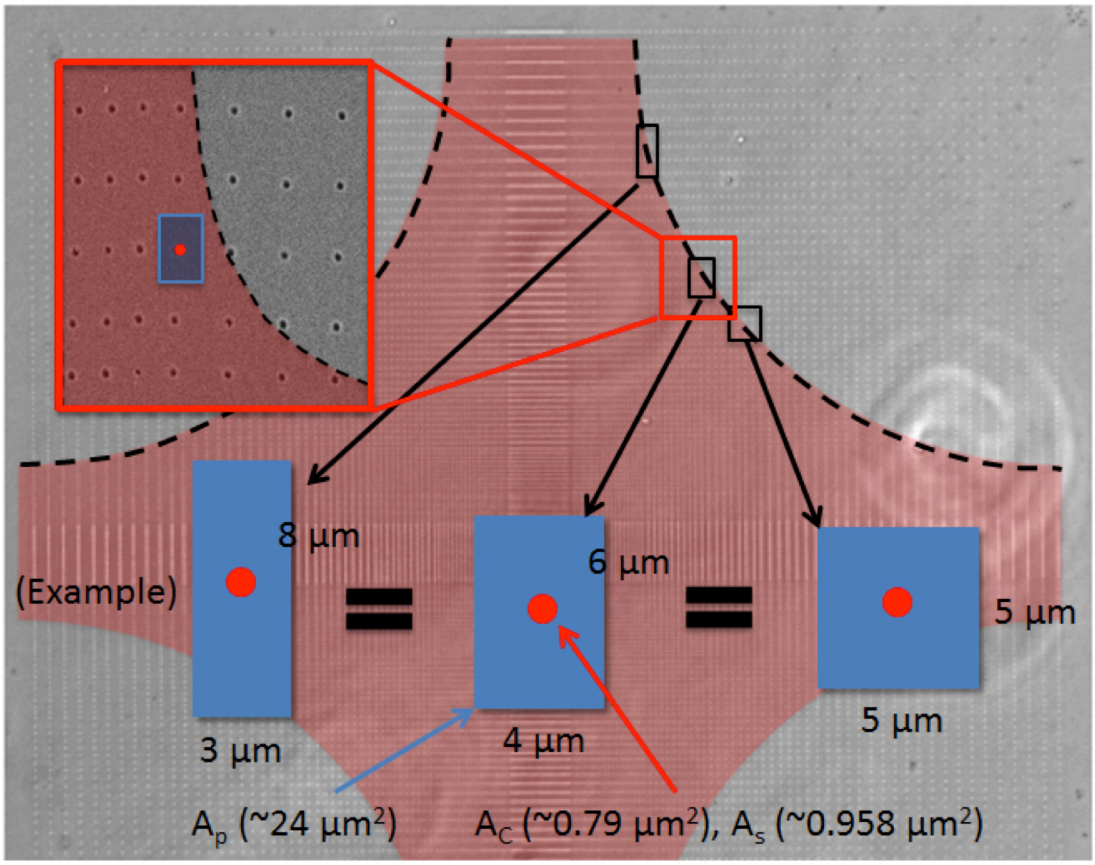

Figure S6. Cell repelling zone (red colored area) and boundary lines (black dashed lines) are overlaid an image of the gradient pattern. The same Surface Area Index (**SAI**) applies to cells along the boundary lines. For example, the area of the unit plane surface (A_p), area of a crater opening (A_c), and surface area inside the crater (A_s) are about 24 μm ^{2}, 0.785 μm ^{2}, and 0.958 μm ^{2}, respectively, for the case of 6 μm x 4 μm unit cell area with 1000-nm diameter and 350-nm depth patterns. The SAI is 0.032. An inset with red border shows the magnified image around 6 μm x 4 μm unit cell area and the boundary line. **SAI**: area of a crater opening (A_c) / (area of a unit plane surface (A_p) - area of a crater opening (A_c) + surface area inside the crater (A_s))

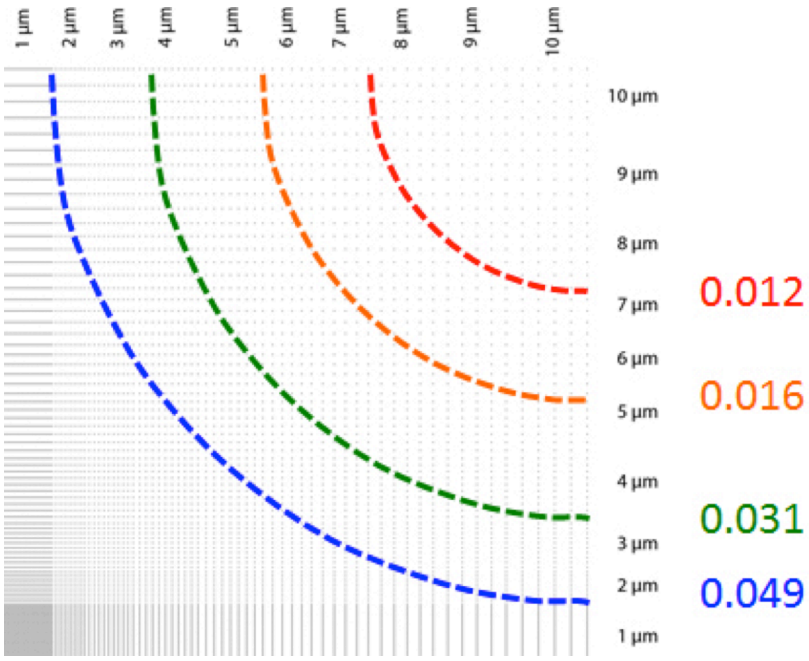

Figure S7. Schematic showing boundary lines of isometric Surface Area Index (SAI) for the case of 1000-nm diameter and 350-nm depth patterns.

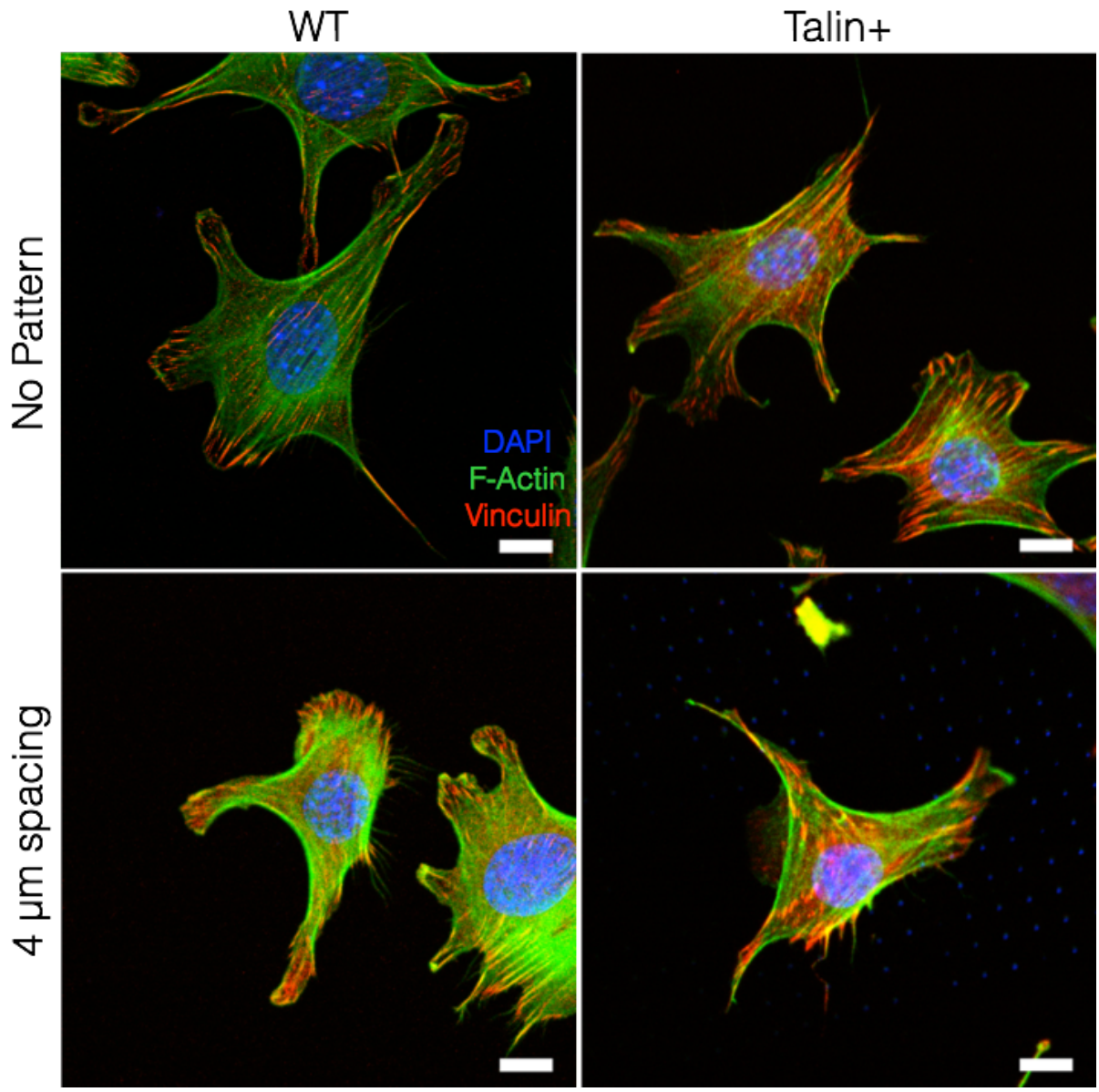

Figure S8. Talin-1(405) transfection encourages focal adhesion maturation. Immunofluorescence images of fibroblasts transfected with Talin-1(405) cultured on isometric patterned surfaces (quartz) with craters of 1 μm in diameter and 350 nm in depth. Transfection with Talin-1(405) plasmids increased over focal adhesion formation throughout the cell body. Cells on patterns have focal adhesions concentrated in the leading and trailing edges that are much larger and mature in size than in wild type cells. Scale bars =10 μm.

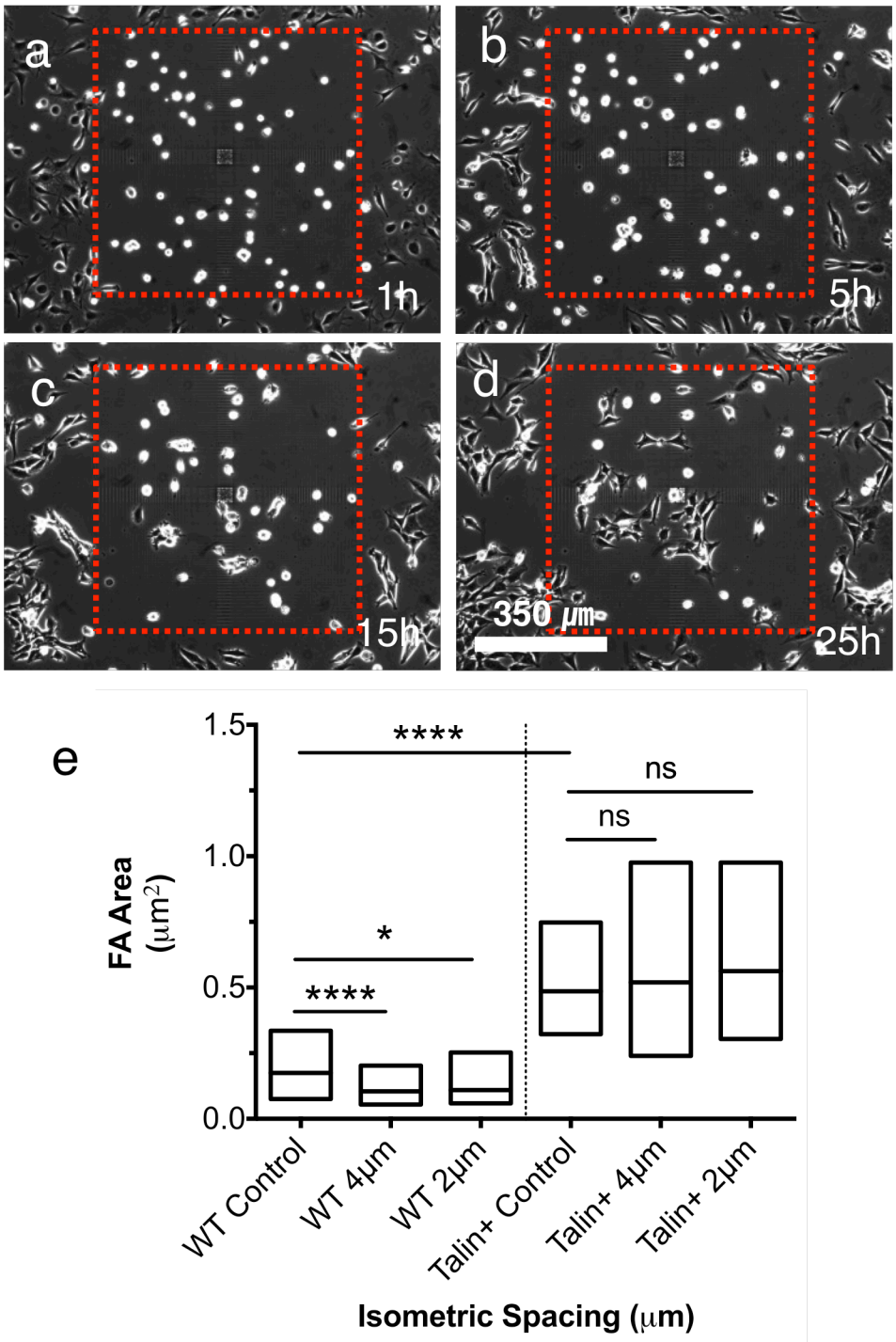

Figure S9. Time-lapse phase-contrast images of Talin-1(405) transfected NIH3T3 cells cultured on a spacing-gradient pattern (quartz). **a-d,** The distance between features varied between 1 and 10 µm, detailed dimensions are shown in Supplementary Fig. S5. The gradient was patterned on an area of 700 × 700 μm^2 with crater diameter and depth of 1000 nm and 350 nm (red dotted-line square). **e,** Talin-1(405) transfected cells showed significantly larger focal adhesion area compared to wild type cells. The cells were fixed 1 hour after seeding. Control surfaces were unpatterned. ns = p>0.05,*p≤ 0.05,**p≤ 0.01, ***p≤0.001, ****p≤0.0001 (Kruskal-Wallis).

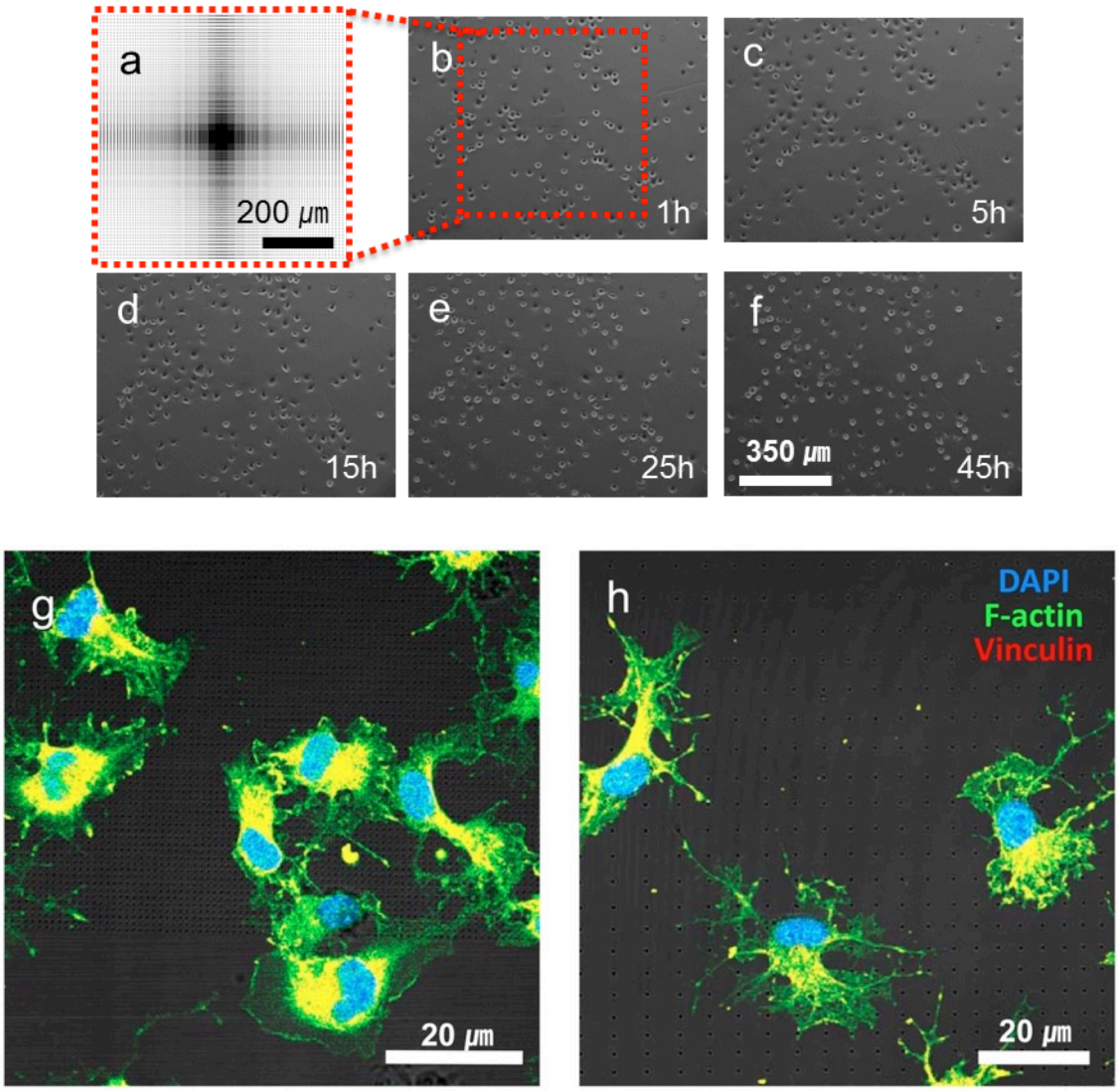

Figure S10. a-f, Time-lapse phase-contrast images of fibroblast cells on the spacing-gradient patterns (quartz) in medium containing 50 μM Blebbistatin. Directional migration was not observed. **g,** Immunofluorescence image of fibroblasts on isometric pitch (2 μm) pattern of quartz in medium containing 50 μM Blebbistatin. **h**, Immunofluorescence image of fibroblasts on spacing-gradient pattern of quartz in medium containing 50 μM Blebbistatin. The dendric extensions appeared with deficient stress cytoskeletal fibers and focal adhesions. F-actin in green, Vinculin in red, DAPI in blue.

To prevent cell spreading while still allowing adhesion, we treated the cells with blebbistatin. Blebbistatin is a small molecule inhibitor with high affinity to myosin II that hinders binding of myosin II to actin. This binding interference results in the inhibition of myosin II contractility and cell migration. Cells seeded on the quartz patterns and treated with 50μM blebbistatin developed dendritic extensions with deficient stress fibers and focal adhesions but did not migrate (Fig. S10). They adhered and remained at one position without significant movement (migration speed ≈ 0). Hence, distinct physical data such as migration speed, motility coefficient (≈ 0), persistent time (≈ infinite) and persistent distance (≈ 0) were non-existent. This finding confirms that the observed cell repellant effect is indeed due to migration and not to adhesion.

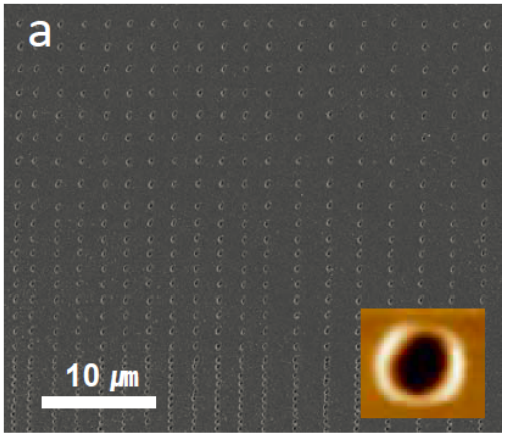

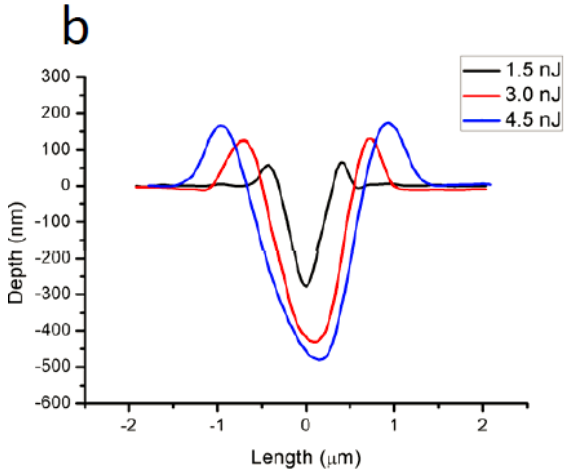

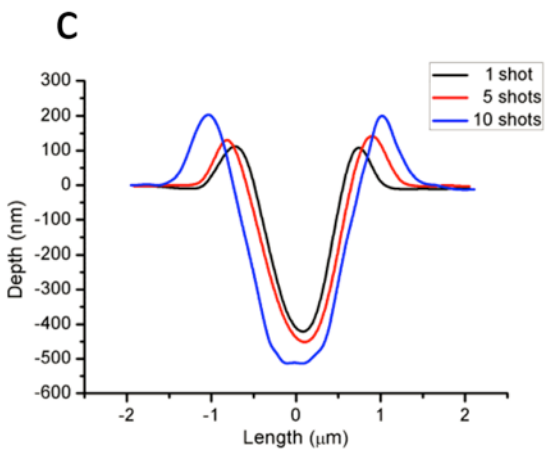

d

Diameter (nm)	Depth (nm)	Height of lip (nm)	FWHM of lip (nm)	Laser power (nJ)	Number of Laser pulses
690	250	30	82	1.5	1
1100	420	120	140	3	1
1500	480	150	400	4.5	1
1230	450	140	275	3	5
1500	500	200	470	3	10

Figure S11. Nanoscale craters on TCPS were fabricated by direct-laser ablation lithography by 50x objective lens. **a,** SEM image of patterned crater. The inset shows an AFM scan of one ablated pattern. **b,** Cross sectional profiles at the centerline of the ablated nanocraters depending on pulse energies with a single pulse using 50x objective. **c,** Cross sectional profiles at the centerline of the ablated nanocraters depending on number of laser pulses with specific (3nJ) laser power. **d,** Dimensions of nanocraters in the ablated patterns on TCPS surfaces. FWHM: Full width at half maximum

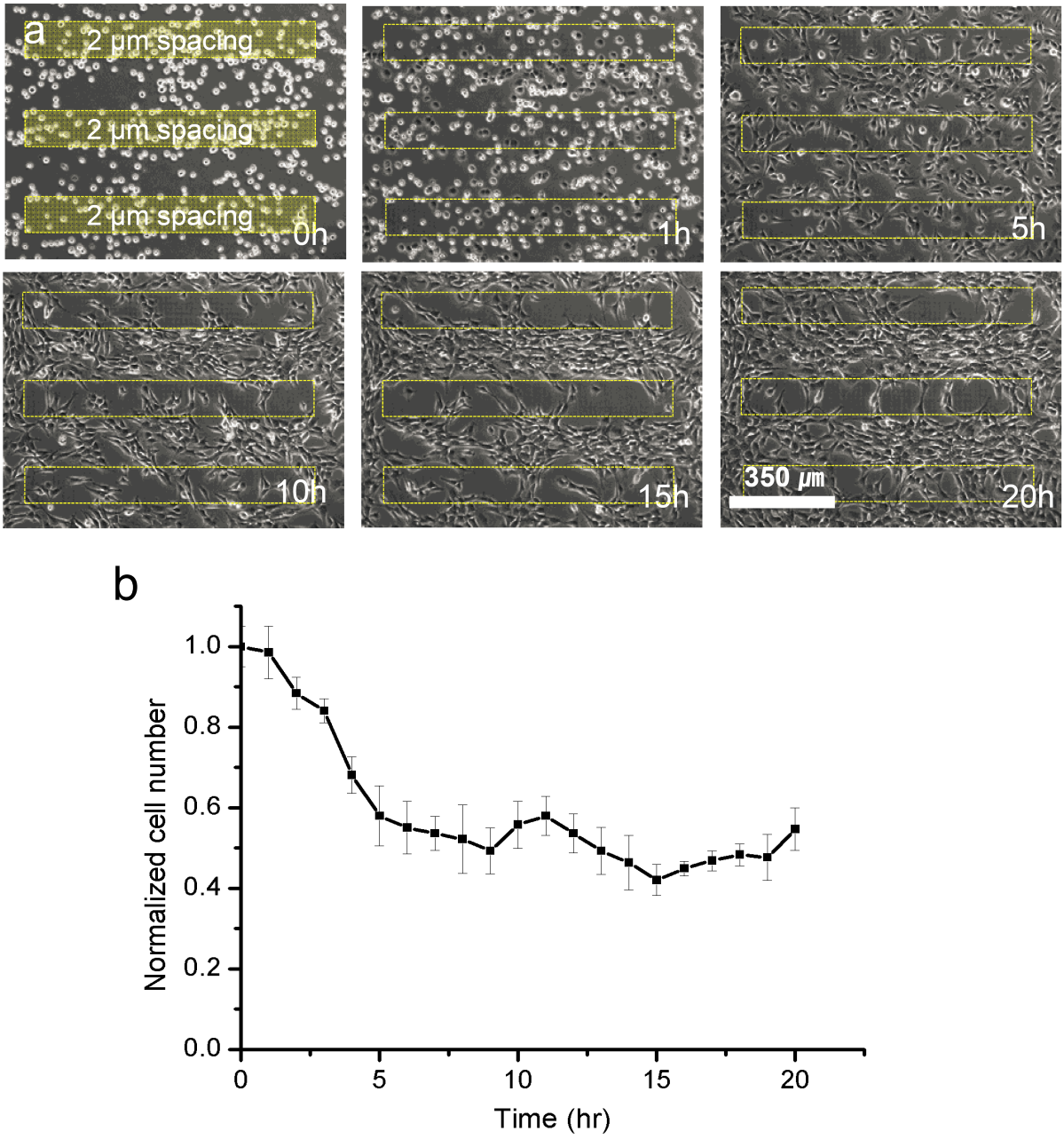

Figure S12. a, Time-lapse phase-contrast images of NIH3T3 cells cultured on isometric pitch (2 **μ**m) patterns (TCPS) with 1100-nm diameter and 420-nm depth nanocraters. After 10 hours from initial cell seeding, we could observe distinct cell patterning. **b,** A plot of the normalized cell number (cell number / initial cell number) shows the repellent effect on the 2-μm spacing patterned area.

Due to the polymer-laser interaction, nanocraters in TCPS were surrounded by a lip (Fig. S11b), which prevented the fabrication of pattern with pitches less than 2 μm. We prepared patterned samples with isometric pitches of 2, 4, 6, and 8 μm, similar to Fig. 2. On the 2-μm spacing area, a cell repellent effect similar to the one on quartz was observed as cells migrated away from the ablated region (Fig. S12). On the 4, 6 and 8-μm spacing area no directional migration or repellent effect could be observed, which we attribute to the increased roughness due to the lip and thereby enlarged available area for focal adhesions.

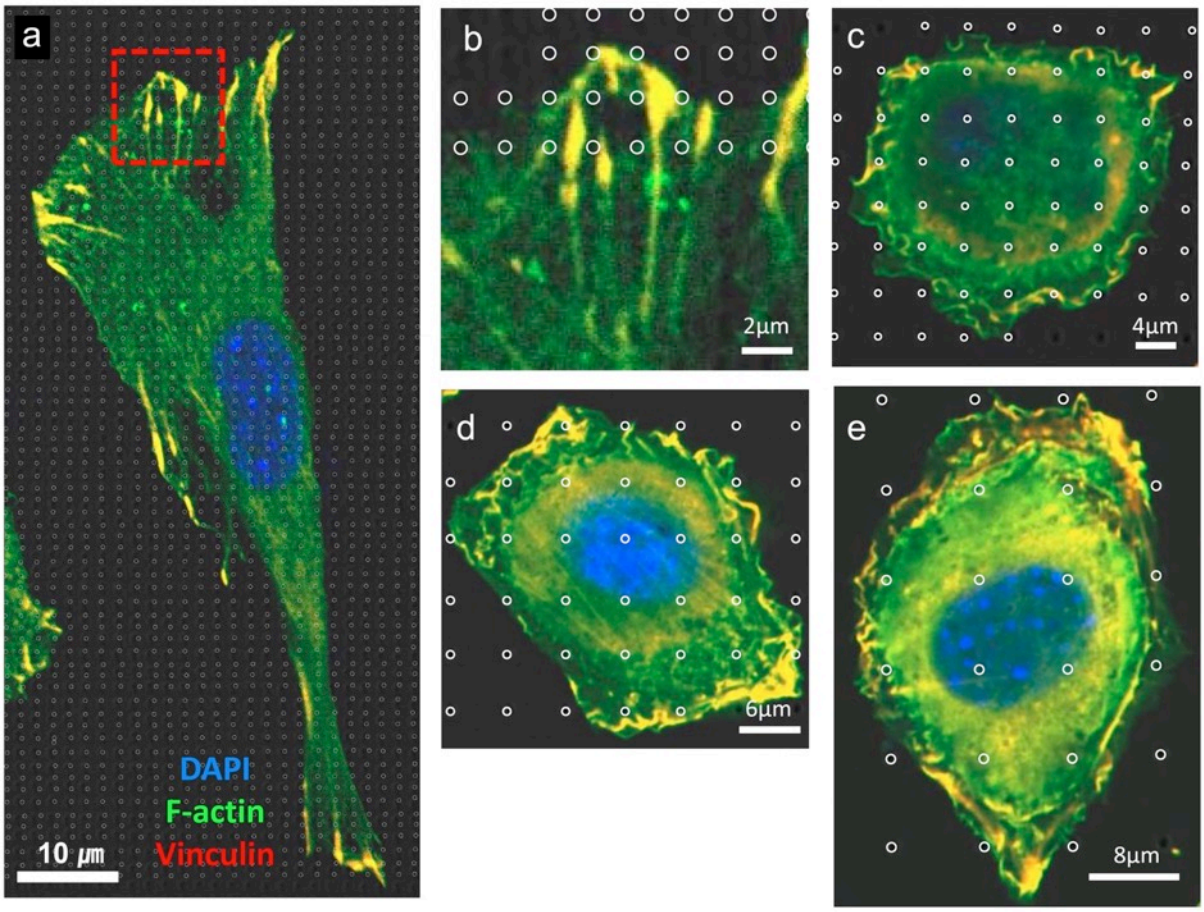

Figure S13. a, Immunofluorescence image of fibroblasts on isometric pitch (2 μm) patterns of TCPS. **b,** Red inset from a showing focal adhesion distribution imaged through vinculin staining. **c-e,** Immunofluorescence image of cells on different isometric pitch 4, 6 and 8 μm pitch pattern respectively. Distribution of focal adhesion on these patterns doesn't show significant directionality. F-actin in green, Vinculin in red, DAPI in blue.

On the patterned quartz surfaces, cells revealed different morphology and focal adhesion distribution depending on pattern pitch. Cells on surfaces with the smallest pitch had smaller and less pronounced focal adhesions that were primarily distributed at the leading and trailing edges of cells. On the patterned TCPS surfaces, we also observed different focal adhesion formation depending on the pattern spacing (Fig. S13). Focal adhesions located on 2-μm pitch isometric pattern were distributed at the leading and trailing edges of cells, and appeared less mature compared to those on the larger pitch patterns with larger planar areas. These results are similar to Figure 5, but the 2-μm pitch patterns on TCPS seem more mature than on quartz. This again can be explained due to the enlargement of the available area for focal adhesions by the topography of the lip, which basically calls for a comparison of the 2-μm pitch TCPS patterns to the larger pitch patterns on quartz. This finding, however, goes in line with our conclusion that the cell repellant effect stems from the disruption of the maturation of focal adhesions by limitation of the available planar area. Whereby the latter is given by the pattern pitch and the topography in between craters.

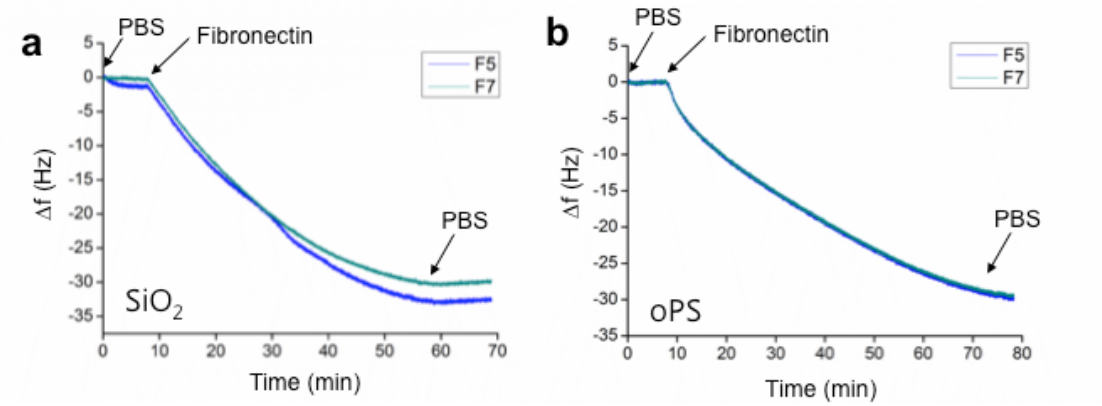

Figure S14. QCM-D measurement of fibronectin adsorption on SiO_2 and oxidized polystyrene (oPS). Frequency shift data for adsorption to **a** SiO_2 and **b** O_2-plasma-treated Polystyrene.

Protein adsorption at interfaces is influenced by the surface chemistry of the material. In order to further characterize the adsorption kinetics of fibronectin on both surfaces, we performed QCM-D measurements using SiO_2 and O_2 plasma-treated Polystyrene (oPS) sensors (Fig. S14). Both surfaces yielded comparable results regarding frequency shifts after 50min incubation indicating a similar mass of fibronectin on both surfaces. The Δf values on the SiO_2 surfaces were 30 Hz, and adsorption to oPS resulted in a shift of 29.5 Hz.

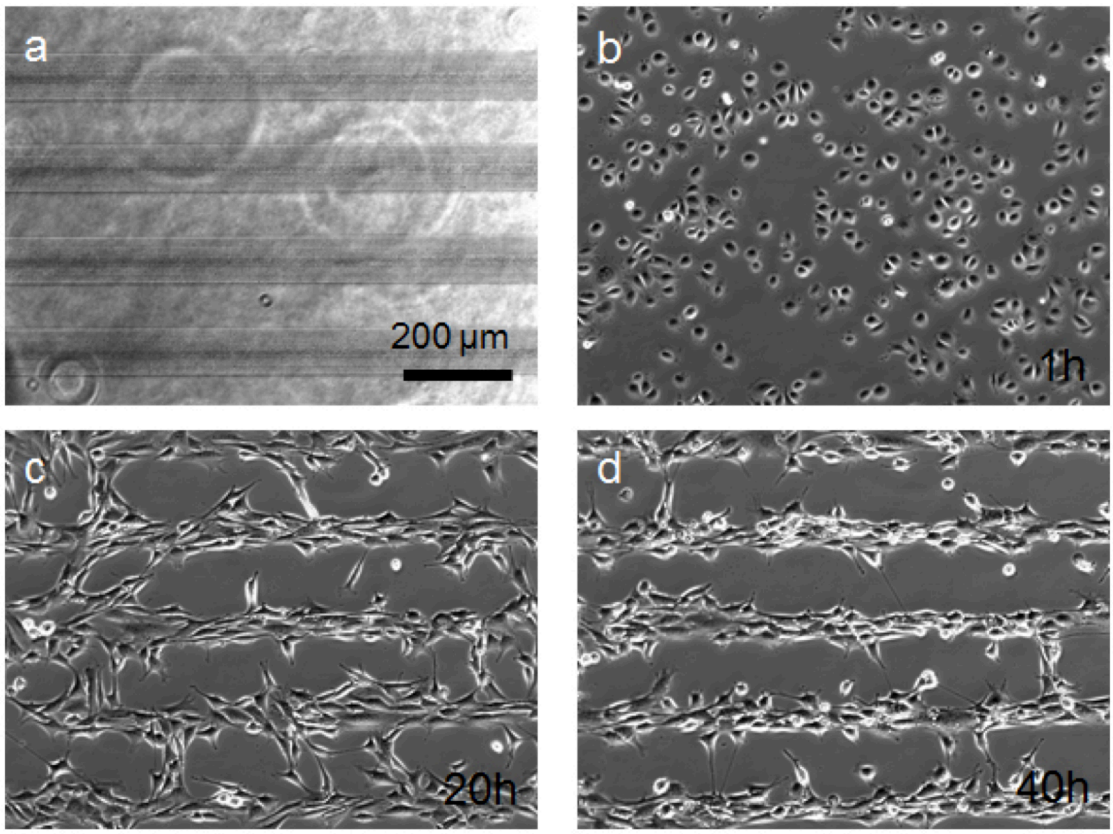

Figure S15. Formation of cell stripes by multiple arrays of nanoscale topographical patterns (quartz, 1000 nm in diameter and 350 nm in depth) 40 hours after cell seeding. **a,** To examine the efficiency of the cell repellant surfaces, we fabricated gradient patterns (from 2 μm (center), to 4 μm (borders)) in 150-μm × 2000-μm areas, of which the SAI at the edges of the patterns was 0.09. **b-d,** Cells migrated from the patterned area and towards planar surfaces, resulting in striped patterns of cells.

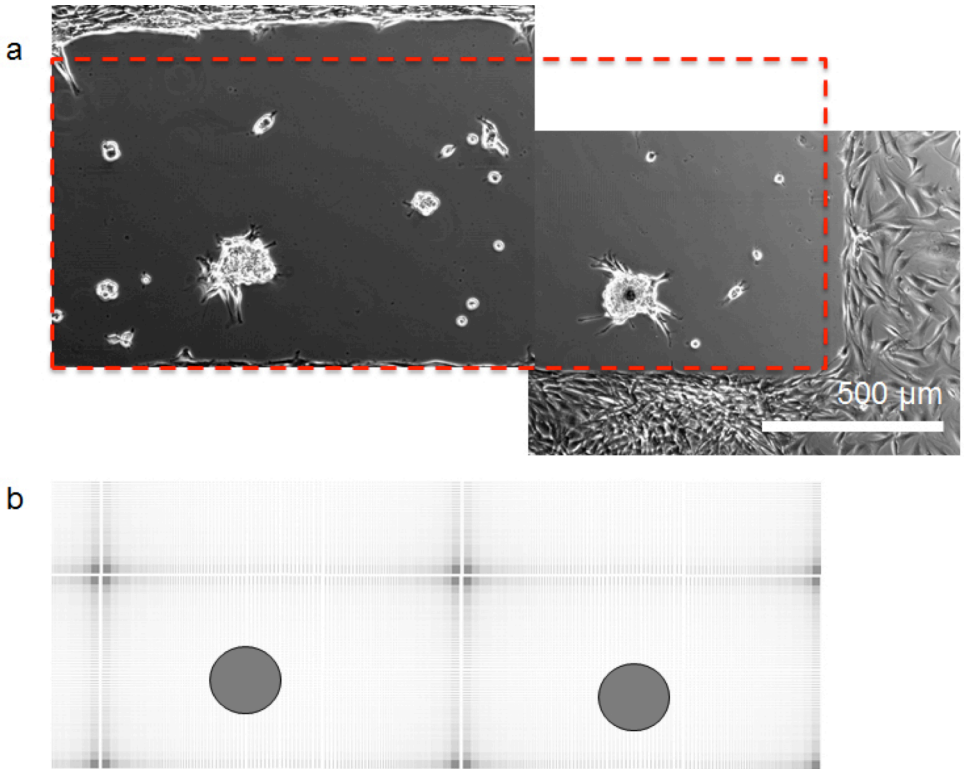

Figure S16. a, Formation of cell clusters formed by an array of gradient patterns (quartz, 1000 nm in diameter and 350 nm in depth) 24 hours after cell seeding. **b,** Schematic diagram of patterned area indicating the locations of cell clusters inside of the box of **a**.

Supplementary Movie Legends

Supplementary Movie 1.
Phase-contrast time-lapse movie of NIH3T3 cells cultured on isometric pitch (2 and 4 μm) patterns and a spacing gradient (2, 3, and 4 μm) pattern with 800-nm diameter and 300-nm depth nanocraters during 25 hours.

Supplementary Movie 2.
Phase-contrast time-lapse movie of cell migration on spacing gradient patterns of 1000 nm in diameter and 350 nm in depth during 25 hours.

Supplementary Movie 3.
Phase-contrast time-lapse movie of cell migration on spacing gradient patterns of 600 nm in diameter and 350 nm in depth during 25 hours.

Supplementary Movie 4.
Phase-contrast time-lapse movie of cell migration on spacing gradient patterns of 1000 nm in diameter and 100 nm in depth during 25 hours.

Supplementary Movie 5.
Phase-contrast time-lapse movie of cell clustering on spacing gradient patterns of 1000 nm in diameter and 350 nm in depth during 22 hours.